^{1}H NMR Investigations of Triphenylporphyrin Metal Complexes and Electronic Interactions in Iron(III) Complexes of *meso*−*meso*-Linked 5,5′-Bis(10,15,20-triphenylporphyrin)

Jacek Wojaczyński, Lechosław Latos-Grażyński,* Piotr J. Chmielewski, Pamela Van Calcar, and Alan L. Balch

Department of Chemistry, University of Wrocław, 14 F. Joliot-Curie Street, Wrocław 50 383, Poland, and Department of Chemistry, University of California, Davis, California 95616

Received January 6, 1999

The ^{1}H NMR spectra of iron(III) complexes of dimeric 5,5′-bis(10,15,20-triphenylporphyrin) [$(TrPPH_2)_2$], 5,5′-bis(10,15,20-tris(*p*-methoxyphenyl)porphyrin) [$(Tr(p\text{-}MeOP)PH_2)_2$], and hybrid $(TrPPH_2)(Tr(p\text{-}MeOP)PH_2)$ and the respective monomeric 5,10,15-triphenylporphyrin ($TrPPH_2$) and 5,10,15-tris(*p*-methoxyphenyl)porphyrin [$Tr(p\text{-}MeOP)PH_2$] have been investigated in order to elucidate an impact of a direct *meso*−*meso* linkage on the electronic structure of corresponding high- and low-spin iron(III) porphyrins. The following species, covering the representative spin/oxidation states, have been investigated: $(TrPP)_2(Fe^{III}Cl)_2$ (high spin); $[(TrPP)_2(Fe^{III}(CN)_2)_2]^{2-}$ (low spin); $[(TrPP)_2(Fe^{III}Cl)_2]^+$ (high-spin iron(III), diporphyrin radical); $[(TrPP^{\bullet})_2(Fe^{III}Cl)_2]^{2+}$ (high-spin iron(III), diradical of diporphyrin). The iron(III) diporphyrins $(TrPP)_2(Fe^{III}Cl)_2$, $[(TrPP)_2(Fe^{III}(CN)_2)_2]^{2-}$, $\{[(TrPP)Fe^{III}(CN)_2][(Tr(p\text{-}MeOP)P)Fe^{III}(CN)_2]\}^{2-}$, and $[(TrPP)_2(Fe^{III}Cl)_2]^{2+}$ revealed the ^{1}H NMR features which have been typically encountered in the spectra of the relevant monomeric complexes. Thus magnetic interactions between two subunits via skeleton appear to be minor. The characteristic broadening and/or paramagnetic shifts of 3-H and 7-H resonances were determined and are diagnostic features of the *meso*−*meso* linkage. One-electron, ligand-based oxidation of $(TrPP)_2(Fe^{III}Cl)_2$ to produce $[(TrPP)_2(Fe^{III}Cl)_2]^+$ was observed with the unpaired electron delocalized over both macrocycles. The structure of $(Tr(p\text{-}MeOP)P)Zn^{II}\cdot 0.4CH_2Cl_2$, the fundamental building block in synthesis of diporphyrins, was determined by X-ray crystallography. $(Tr(p\text{-}MeOP)P)Zn^{II}$ crystallizes in the monoclinic space group $C2/c$ with $a = 47.744(9)$ Å, $b = 9.090(2)$ Å, $c = 15.571(2)$ Å, $\beta = 93.770(13)°$, and $Z = 8$. The refinement of 494 parameters and 4361 reflections yields $R_1 = 0.0756$, $wR_2 = 0.2169$. The $(Tr(p\text{-}MeOP)P)Zn^{II}$ presents characteristic features of zinc(II) tetraphenylporphyrin. The molecular periphery of $(Tr(p\text{-}MeOP)P)Zn^{II}$ has a fully exposed *meso* position and two partially exposed pyrrole rings.

Introduction

Oligomeric porphyrins and metalloporphyrins of various structures are under intensive investigation due to their relevance to the mechanism of photosynthesis and their potential application in the molecular electronics and as new photonic materials.[1−3] For instance, the spectacular photonic molecular wires based on side-by-side oligomerization of *meso*-functionalized porphyrins have been shown to absorb light at one end and then to emit a different photon on the other end.[4] Other studies of oligomeric metalloporphyrins were directed toward generation of artificial allosteric systems.[5] Polymetalloporphyrins were investigated as polyelectron redox molecular catalysts in the four-electron reduction of dioxygen[6] or in proton reduction.[7]

In general, distance, geometry, and orientation have been recognized as important factors for control of the efficiency of the energy and electron-transfer processes.[1] Therefore, oligomeric porphyrins in which π-systems can directly interact have particular interest. Crossley and co-workers described a synthetic approach to molecular wires based on rigid π-conjugated porphyrins that are bridged by a coplanar aromatic fragment. Theoretical analysis of the conjugation pathway for oligoporphyrins connected by 1,4,5,8-tetrazaantracene moieties suggests that the interaction between the porphyrins and the aromatic bridge is weak contrary to the anticipated aromatic π-delocalization.[2,8] Recently a conjugated oligoporphyrin system based on fused pyrrole blocks has been synthesized by Smith and coworkers.[9]

* To whom correspondence should be addressed

(1) (a) Wasielewski, R. *Chem. Rev.* **1992**, *92*, 435. (b) Gust, D.; Moore, T. A. *Topics in Current Chemistry*; Springer-Verlag: Berlin, 1991; Vol. 159, pp 103−156.
(2) (a) Crossley, M. J.; Burn, P. L. *J. Chem. Soc., Chem. Commun.* **1987**, 39. (b) Crossley, M. J.; Burn, P. L. *J. Chem. Soc., Chem. Commun.* **1991**, 1569.
(3) (a) Cosmo, R.; Kautz, C.; Meerholz, K.; Heinze, J.; Müllen, K. *Angew. Chem., Int. Ed. Engl.* **1989**, *28*, 604. (b) Lamrabte, A.; Momenteau, M.; Maillard, P.; Seta, P. *J. Mol. Electron.* **1990**, *6*, 145. (c) Ono, N.; Tomita, H.; Maruyama, K. *J. Chem. Soc., Perkin Trans. 1* **1992**, 2453.
(4) Wagner, R. W.; Lindsey, J. S. *J. Am. Chem. Soc.* **1994**, *116*, 9759. (b) Anderson, H. L.; Martin, S. J.; Bradley, D. D. C. *Angew. Chem., Int. Ed. Engl.* **1994**, *33*, 655.
(5) Tabushi, I. *Pure Appl. Chem.* **1988**, *60*, 581.
(6) (a) Ni, C.-L.; Abdalmuhdi, I.; Chang, C. K.; Anson. F. C. *J. Phys. Chem.* **1987**, *91*, 1158. (b) Collman, J. P.; Hutchison, J. E.; Lopez, M. A.; Tabard, A.; Guilard, R.; Seok, W. K.; Ibers, J. A.; L'Her, M. *J. Am. Chem. Soc.* **1992**, *114*, 9689.
(7) Collman, J. P.; Ha, Y.; Wagenknecht, P. S.; Lopez, M.-A.; Guilard, R. *J. Am. Chem. Soc.* **1993**, *115*, 9080.
(8) Crossley, M. J.; Burn, P. L.; Chew, S. S.; Cuttance, F. B.; Newsom, I. A. *J. Chem. Soc., Chem. Commun.* **1991**, 1564. (b) Crossley, M. J.; Burn, P. L.; Langford, S. J.; Pyke, S. M.; Stark, A. G. *J. Chem. Soc., Chem. Commun.* **1991**, 1567. (c) Lü, T. X.; Reimers, J. R.; Crossley, M. J.; Hush, N. S. *J. Phys. Chem.* **1994**, *98*, 11878. (d) Crossley, M. J.; Govenlock, L.; J.; Prashar, J. K. *J. Chem. Soc., Chem. Commun.* **1995**, 2379.

10.1021/ic990038g CCC: $18.00
Published on Web 05/29/1999

An alternative approach to construct the porphyrin array with strongly interacting π-electron systems involves the formation of direct links between *meso*-carbons without any spacer element.[10] Such molecules have been recently synthesized via oxidative coupling of zinc porphyrins. Up to eight porphyrinic moieties have been linked in this fashion to create linear arrays. A stepwise process has been reported in which the bridging *meso*−*meso* fragment was initially synthesized and subsequently incorporated into the bis-macrocycle.[10d]

The extent of the coupling between porphyrin moieties within oligomeric porphyrins, in which the π-electron systems are expected to interact, remains a major concern. We have decided to explore this issue for iron(III) complexes of 5,5′-linked diporphyrins obtained from *meso*-triaryl-substituted porphyrins.

^{1}H NMR spectroscopy has been shown to be uniquely definitive method for detecting and characterizing iron porphyrins. The hyperfine shift patterns that have been recorded for such paramagnetic complexes are sensitive to the iron oxidation, spin and ligation state.[11] Particularly pyrrole protons

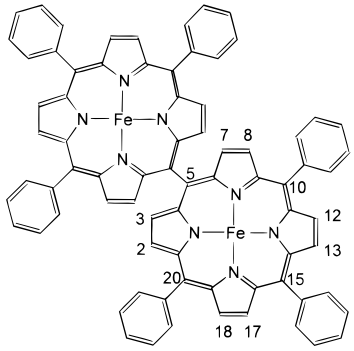

provided a direct probe of the spin density around the porphyrin macrocycle. Previously we have investigated the specific mode of the tetraphenylporphyrin modifications (β-substitution, a selective symmetrical extension of a single pyrrole ring, replacement of *meso*-aryls by *meso*-alkyl substituents).[12] In related spectroscopic investigations on trimeric or dimeric paramagnetic [(2-O-TPP)Fe^{III}]$_3$, [(2-O-TPP)Mn^{III}]$_3$, [(2-O-TPP)-Fe^{III}]$_n$[(2-O-TPP)Mn^{III}]$_{3-n}$, [(OEPO)Fe^{III}]$_2$, and [(OEPO)Fe^{III}]$_2^+$ complexes we have established the ^{1}H NMR "fingerprint"

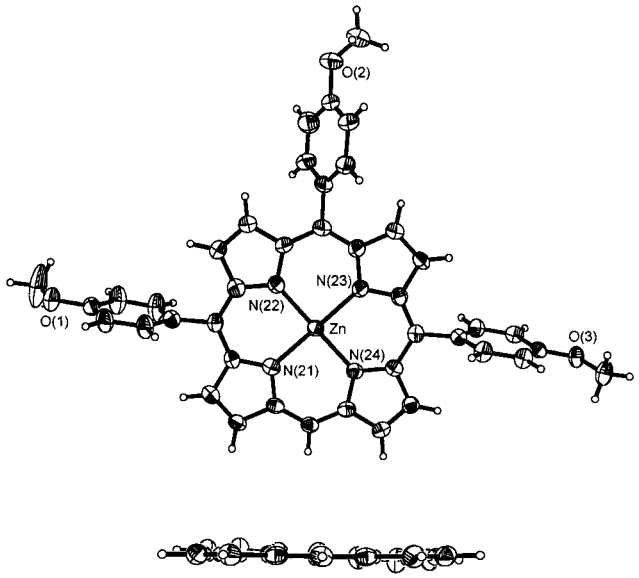

Figure 1. A perspective view (with 50% probability ellipsoids) of (Tr(*p*-MeOP)P)Zn^{II}. The lower drawing emphasizes the planarity of the macrocycle.

evidence of oligomerization.[13−15] Specially, the paramagnetic shift of the 3-H resonance of [(2-O-TPP)M^{III}]$_3$ reflects simultaneous contributions to contact shifts derived from two neighboring paramagnetic metal centers.[14]

This work is concerned with the ^{1}H NMR characterization of high- and low-spin iron(III) complexes of hexa-*meso*-phenyl-substituted *meso*−*meso*-linked diporphyrins. We have found that the ^{1}H NMR spectroscopic properties of the dimeric complexes resemble those of the isolated subunit, i.e., iron(III) 5,10,15-triphenylporphyrin, in analogous spin/electronic states.

Results and Discussion

Synthesis of Diporphyrins and Their Complexes. 5,10,15-Triphenylporphyrin, (TrPPH$_2$) and 5,10,15-tris(*p*-methoxyphenyl)porphyrin (Tr(*p*-MeOP)PH$_2$) have been synthesized in 5−7% yield by the condensation of pyrrole, benzaldehyde (or *p*-methoxybenzaldehyde), and paraformaldehyde. The procedure followed the methodology typically used for synthesis via a mixed aldehyde−pyrrole condensation.[16] The (Tr(*p*-MeOP)P)-Zn^{II} complex has been characterized by X-ray crystallography (Figure 1). As expected, the molecular periphery of (Tr(*p*-MeOP)P)Zn^{II} has a fully exposed *meso* position and two partially exposed pyrrole rings. Thus the molecule periphery presents blending of structural features which are typical for (TPP)Zn^{II} and (OEP)Zn^{II}. The bond lengths and angles are within the limits expected for zinc(II) porphyrins (Table 1).[17] The porphyrin macrocycle is practically flat. The zinc(II) ion is located in the porphyrin plane.

The (TrPP)Zn^{II} complex undergoes a regiospecific *meso*−*meso* coupling mediated by a two-electron oxidizing reagent,

(9) Jaquinod, L.; Siri, O.; Khoury, R. G.; Smith, K. M. *Chem. Commun.* **1998**, 1261.

(10) (a) Susumu, K.; Shimidzu, T.; Tanaka, K.; Segawa, H. *Tetrahedron Lett.* **1996**, *37*, 8399. (b) Osuka, A.; Shmidzu, H. *Angew. Chem., Int. Ed. Engl.* **1997**, *36*, 135. (c) Yoshida, N.; Shimidzu, H.; Osuka, A. *Chem. Lett.* **1998**, 55. (d) Khoury, R. G.; Jaquinoid, L.; Smith, K. M. *Chem. Commun.* **1997**, 1057. (e) Ogawa, T.; Nishimoto, Y.; Yoshida, N.; Ono, N.; Osuka, A. *Chem. Commun.* **1998**, 337. (f) Nakano, A.; Osuka, A.; Yamazaki, I.; Yamazaki, T.; Nishimura, Y. *Angew. Chem., Int. Ed. Engl.* **1998**, *37*, 135.

(11) (a) La Mar, G. N.; Walker, F. A. in *The Porphyrins*, Dolphin, D., Ed.; Academic Press: New York, 1979; pp 61−312. (b) Bertini, I., Luchinat, C. *NMR of Paramagnetic Molecules in Biological Systems*; The Benjamin/Cummings Publishing Co.: Reading, MA, 1986. (c) Bertini, I.; Luchinat, C. *Coord. Chem. Rev.* **1996**, *150*, 131. (d) Walker F. A., Simonis U. In *Biological Magnetic Resonance, Volume 12: NMR of Paramagnetic Molecules*; Berliner L. J., Reuben J., Eds.; Plenum Press: New York, 1993; p 133.

(12) (a) Wojaczyński, J.; Latos-Grażyński, L.; Hrycyk, W.; Pacholska, E.; Rachlewicz, K.; Szterenberg, L. *Inorg. Chem.* **1996**, *35*, 6861. (b) Wojaczyński, J.; Latos-Grażyński, L.; Głowiak, T. *Inorg. Chem.* **1997**, *36*, 6299. (c) Wołowiec, S.;. Latos-Grażyński, L.; Mazzanti, M.; Marchon, J.-C. *Inorg. Chem.* **1997**, *36*, 5761. (d) Wołowiec, S.; Latos-Grażyński, L.; Toronto, D.; Marchon, J.-C. *Inorg. Chem.* **1998**, *37*, 724. (e) Mazzanti, M.; Marchon, J.-C.; Wojaczyński, J.; Wołowiec, S.; Latos-Grażyński, L.; Shang, M.; Scheidt W. R. *Inorg. Chem.* **1998**, *37*, 2476.

(13) (a) Wojaczyński, J.; Latos-Grażyński, L. *Inorg. Chem.* **1995**, *34*, 1044. (b) Wojaczyński, J.; Latos-Grażyński, L. *Inorg. Chem.* **1995**, *34*, 1054. (c) Wojaczyński, J.; Latos-Grażyński, L. *Inorg. Chem.* **1996**, *35*, 4812. (d) Wojaczyński, J.; Latos-Grażyński, L.; Olmstead, M. M.; Balch, A. L. *Inorg. Chem.* **1997**, *36*, 4548.

(14) Balch, A. L.; Latos-Grażyński, L.; Noll, B. C.; Olmstead, M. M.; Zovinka, E. P. *Inorg. Chem.* **1992**, *31*, 2248.

(15) Balch, A. L.; Latos-Grażyński, L.; St. Claire, T. *Inorg. Chem.* **1995**, *34*, 1395.

(16) Lindsey J. S. In *Metallopophyrins Catalyzed Oxidations*; Montanari, F., Casella, L., Eds.; Kluwer Academic Publishers: Netherlands 1994; p 49.

Scheme 1

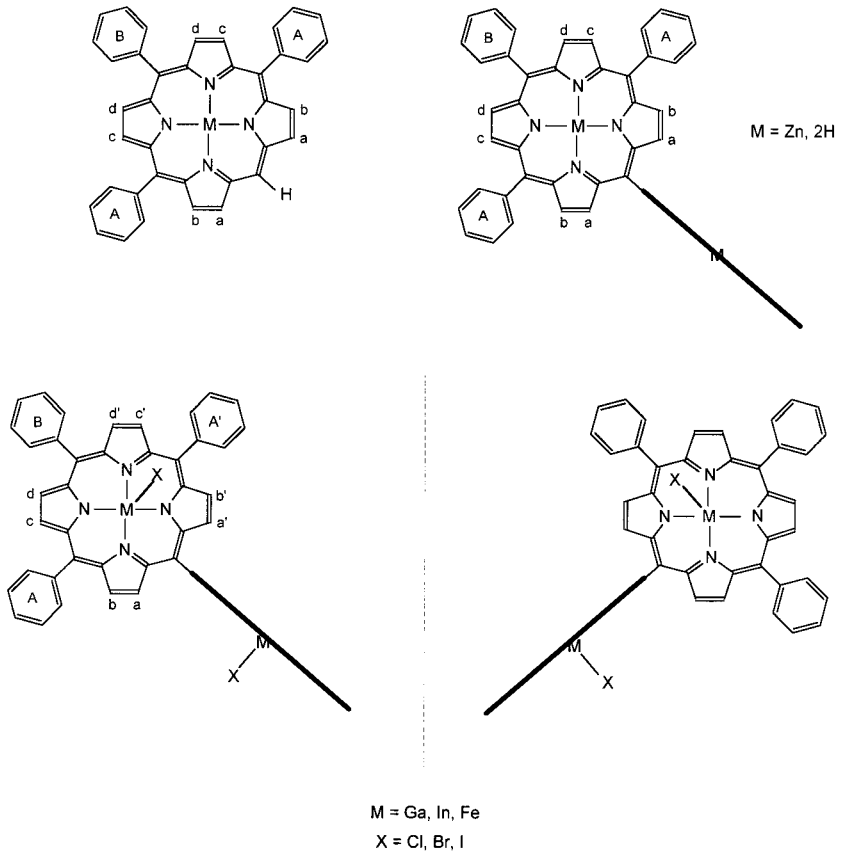

thallium(III) trifluoroacetate (TTFA), to produce zinc(II) 5,5′-bis(10,15,20-triphenylporphyrin) [$(TrPP)_2Zn^{II}_2$], described previously.[10] The coupling procedure performed with a mixture of $(TrPP)Zn^{II}$ and $(Tr(p\text{-}MeOP)P)Zn^{II}$ yields three diporphyrin complexes: $(TrPP)_2Zn^{II}_2$, $(Tr(p\text{-}MeOP)P)_2Zn^{II}_2$, and [$(TrPP)Zn^{II}$][$(Tr(p\text{-}MeOP)P)Zn^{II}$]. The last species contains two distinct subunits. Zinc(II) diporphyrins can be easily demetalated by treatment with acid to produce the dimeric free bases $(TrPPH_2)_2$, $(Tr(p\text{-}MeOP)PH_2)_2$, and $(TrPPH_2)(Tr(p\text{-}MeOP)PH_2)$. Subsequently, diporphyrins can be readily metalated with gallium(III) acetyloacetonate or indium(III) chloride to form $(TrPP)_2(Ga^{III}Cl)_2$ or $(TrPP)_2(In^{III}Cl)_2$. The insertion of iron into $TrPPH_2$, $Tr(p\text{-}MeOP)PH_2$, $(TrPPH_2)_2$, $(Tr(p\text{-}MeOP)PH_2)_2$, and $(TrPPH_2)(Tr(p\text{-}MeOP)PH_2)$ resulted in formation of $(TrPP)Fe^{III}Cl$, $(Tr(p\text{-}MeOP)P)Fe^{III}Cl$, $(TrPP)_2(Fe^{III}Cl)_2$, $(Tr(p\text{-}MeOP)P)_2(Fe^{III}Cl)_2$, and [$(TrPP)Fe^{III}Cl$][$(Tr(p\text{-}MeOP)P)Fe^{III}Cl$], respectively.

^{1}H NMR Studies of Diamagnetic Metallodiporphyrins. To understand the spectral data, the structural characteristics of the monomeric and dimeric porphyrins are systematized in Scheme 1. The monomeric triphenylporphyrin unit will have maximal C_{2v} symmetry when the porphyrin has identical ligation on both sides of the porphyrin plane or C_s symmetry when the ligation on either side is different. In both cases four distinct types of pyrrole protons (labeled a−d) and two types of phenyl groups (labeled A and B) are present.

Table 1. Selected Bond Lengths (Å) and Angles (deg) for $(Tr(p\text{-}MeOP)P)Zn^{II}\cdot 0.4CH_2Cl_2$

Zn−N(21)	2.033(5)	N(21)−Zn−N(23)	179.4(2)
Zn−N(22)	2.019(6)	N(22)−Zn−N(24)	180.0(2)
Zn−N(23)	2.041(5)	N(21)−Zn−N(22)	89.4(2)
Zn−N(24)	2.027(5)	N(22)−Zn−N(23)	90.5(2)
		N(23)−Zn−N(24)	89.5(2)
		N(24)−Zn−N(21)	90.7(2)

For a dimeric porphyrin with simple planar coordination in each macrocycle (i.e. for $(TrPP)_2Zn^{II}_2$), the molecule possesses at least the D_2 symmetry. In the drawing of Scheme 1, this dimer is shown with one subunit in the plane of the paper and the other perpendicular to the page and indicated by a thick line. In such a dimer again four distinct types of pyrrole protons (labeled a−d) and two types of phenyl groups (labeled A and B) are present. The analysis carried out for four-coordinate $(TrPP)_2Zn^{II}_2$ holds for the six-coordinate $(TrPP)_2(M^{III}L_2)_2$ as well.

For the dimeric porphyrin with five-coordinate metal centers in each porphyrin, the structure is more complex. The results of molecular mechanics calculations which have been used to visualize the structure of the gallium(III) diporphyrin are shown in Figure 2. The ionic radius and the charge of gallium(III) (and of indium(III) and high-spin iron(III) as well) impose five-coordinate square-pyramidal structures on each $(TrPP)Ga^{III}Cl$ subunit. Accordingly, these metal ions are displaced from the porphyrin plane. In the minimization procedure we have used the standard MM+ parametrization of the HyperChem program with an exception for the metal ion coordination surroundings where the constraints, reflecting the size of the gallium(III) ion, have been imposed. The characteristic features of gallium(III) tetraphenylporphyrins included a displacement of the ion from the plane of four nitrogens by ca. 0.4 Å and relatively long

(17) (a) Scheidt, W. R.; Mondal, J. U.; Eigenbrot, C. W.; Adler, A.; Radonovich, L. J.; Hoard, J. L. *Inorg. Chem.* **1986**, *25*, 795. (b) Byrn, M. P.; Curtis, C. J.; Khan, S. I.; Sawin, P. A.; Tsurumi, R.; Strouse, C. E. *J. Am. Chem. Soc.* **1990**, *112*, 1865. (c) Byrn, M. P.; Curtis, C. J.; Goldberg, I.; Hsiou, Y.; Khan, S. I.; Sawin, P. A.; Tendick, S. K.; Strouse, C. E. *J. Am. Chem. Soc.* **1991**, *113*, 6549. (d) Byrn, M. P.; Curtis, C. J.; Hsiou, Y.; Khan, S. I.; Sawin, P. A.; Tendick, S. K.; Terzis, A. Strouse, C. E. *J. Am. Chem. Soc.* **1993**, *115*, 9480.

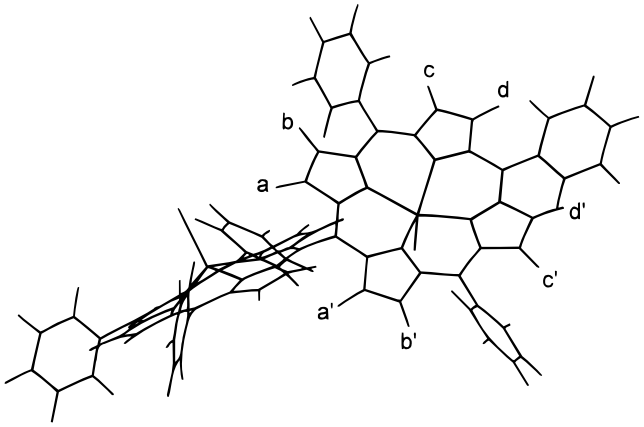

Figure 2. Drawing of $(TrPP)_2(Ga^{III}Cl)_2$ as obtained from the Hyperchem MM+ molecular mechanics calculations. The labels are related to the ^{1}H NMR spectra of $(TrPP)_2(Ga^{III}Cl)_2$ ($(TrPP)_2(M^{III}X)_2$) in the paper.

Ga−N bonds (2.05 Å). The structural parameters are in the range found for a variety of gallium(III) porphyrins by X-ray crystallography.[18,19] The calculations indicate that two subunits of $(TrPP)_2(Ga^{III}Cl)_2$ are not necessarily orthogonal. The dimeric molecule has the C_2 symmetry with the C_2 axis perpendicular to the C(5)−C(5′) bond, and the two $(TrPP)Ga^{III}$ subunits are equivalent. However, as seen in Scheme 1, the pyrrolic positions 7-H(a) and 3-H(a′), 8-H(b), and 2-H(b′), as well as 12-H(c) and 18-H(c′), and 13-H(d) and 17-H(d′) are no longer equivalent as they are in the monomeric $TrPPH_2$ or in $(TrPP)_2Zn^{II}_2$. Additionally, the symmetry lowering in these five-coordinate complexes renders the three phenyl substituents on each porphyrin inequivalent. On each *meso* phenyl ring, the two *ortho* and two *meta* protons are not equivalent because the porphyrin plane bears different substituents on opposite sides and rotation about the *meso*-carbon−phenyl bond is restricted. As an additional complication, five-coordinate $(TrPP)_2(M^{III}Cl)_2$ has an optical asymmetry associated with direction of the axial orientation on the metal(III) ions, as shown in the Scheme 1. The geometric considerations described above for gallium(III) are also relevant for other five-coordinate metals, indium(III), and high-spin iron(III).

Figure 3 shows the ^{1}H NMR spectra of monomeric $(TrPP)Ga^{III}Cl$ and dimeric $(TrPP)_2Zn^{II}_2$, $(TrPP)_2(Ga^{III}Cl)_2$, and $(TrPP)_2(In^{III}Cl)_2$. For $(TrPP)Ga^{III}Cl$, the pyrrole protons produce two AB patterns as expected for the effective C_s symmetry. The mirror plane passes through the gallium(III) ion, the axial chloride, and the unsubstituted *meso*-carbon. Note that in monomeric $(TrPP)Ga^{III}Cl$ the 3,7-H(a) protons have chemical shifts that are downfield of the other pyrrole protons, because they do not experience a ring current shift from an adjacent *meso*-phenyl group. The unique *meso* proton resonance is located at 10.41 ppm.

The ^{1}H NMR spectra of the diporphyrinic complexes reveals the absence of a *meso* proton resonance and unusual chemical shifts of the pyrrole resonances. For $(TrPP)_2Zn^{II}_2$, all of the pyrrole resonances experience an upfield bias with the pyrrole

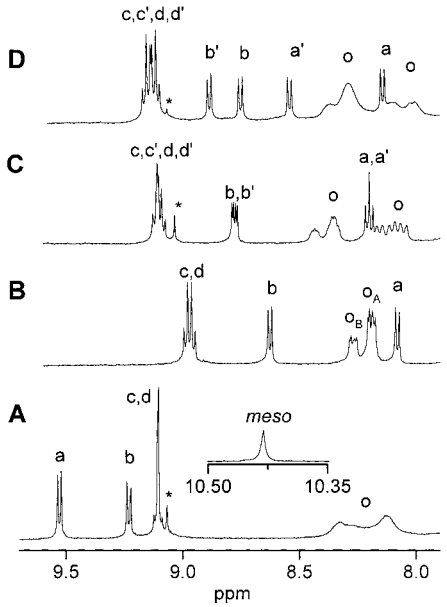

Figure 3. The downfield region of ^{1}H NMR spectra (300 MHz): A, $(TrPP)Ga^{III}Cl$; B, $(TrPP)_2Zn^{II}_2$; C, $(TrPP)_2(In^{III}Cl)_2$; D, $(TrPP)_2(Ga^{III}Cl)_2$. Their assignments correspond to those in Scheme 1 and Figure 2 (o, ortho proton resonances). Some resonances from an admixture of $(TPP)In^{III}Cl$ (trace C) and $(TPP)Ga^{III}Cl$ (traces A and D) marked with asterisks.

resonance furthest upfield assigned to the a type pyrrole protons. The upfield shifts result from the ring current effect of the adjacent macrocycle, as noted earlier.[10]

The geometric differences between the monomeric and dimeric species are further exemplified by comparison of $(TrPP)Ga^{III}Cl$ and $(TrPP)_2(Ga^{III}Cl)_2$. Due to the lower symmetry of the dimer, four different AB patterns are observed in the ^{1}H NMR spectra of $(TrPP)_2(Ga^{III}Cl)_2$ [and in $(TrPP)_2(In^{III}Cl)_2$ as well]. Thus in dimeric molecules the 7-H, 3-H, 8-H, and 2-H (a, a′, b, b′) protons experience large upfield chemical shifts due to their proximity to the π-system of the adjacent porphyrin.

These ^{1}H NMR spectral characteristics are essential since the zinc(II), gallium(III), and indium(III) complexes will be used as the appropriate diamagnetic references for the paramagnetic low-spin and high-spin iron(III) complexes of *meso*−*meso*-linked diporphyrins, respectively. Chemical shift data of these and other diamagnetic compounds are given in Table 2.

High-Spin Iron Porphyrins—^{1}H NMR Studies. Representative ^{1}H NMR spectra of high-spin $(TrPP)Fe^{III}Cl$ and $(TrPP)Fe^{III}I$ complexes are shown in Figure 4. Resonance assignments which are given in Figure 4 and in Table 3 have been made on the basis of relative intensities and line width analysis. Direct comparisons to iron(III) tetraphenylporphyrin derivatives facilitated the assignment.[11,20] The multiplicity of the respective resonances is directly related to the symmetry of the molecule as discussed in detail for the analogous $(TrPP)Ga^{III}Cl$. Thus, the four unequivalent pyrrole positions produce the four downfield shifted pyrrole resonances for well-resolved spectrum of $(TrPP)Fe^{III}I$.

The line width of the pyrrole resonances is practically identical for the four pyrrole lines in the spectrum of $(TrPP)Fe^{III}I$. The line width increases, as expected, in the series $(TrPP)Fe^{III}I < (TrPP)Fe^{III}Br < (TrPP)Fe^{III}Cl$.[11,20] Two of the four pyrrole lines overlap in the case of $(TrPP)Fe^{III}Cl$. These downfield resonances are accompanied by an upfield *meso*

(18) (a) Coutsolelos, A.; Guilard, R.; Boukhris, A.; Lecomte, C. *J. Chem. Soc., Dalton Trans.* **1986**, 1779. (b) Boukhris, A.; Lecomte, A.; Coutsolelos, A.; Guilard, R. *J. Organomet. Chem.* **1986**, *303*, 151. (c) Coutsolelos, A.; Guilard, R.; Bayeul, D.; Lecomte, C. *Polyhedron* **1986**, *5*, 1157. (d) Serr, R., B.; Headford, C. E. L.; Anderson, O. P.; Elliott, C. M.; Spartalian, K.; Fainzilberg, V. E.; Hatfield, W. E.; Rohrs, B. R.; Eaton, S. S.; Eaton, G. R. *Inorg. Chem.* **1992**, *31*, 5450.

(19) Balch, A. L.; Hart, R. L.; Parkin, S. *Inorg. Chim. Acta* **1993**, *205*, 137.

(20) Behere, D. V.; Birdy, R.; Mitra, S. *Inorg. Chem.* **1982**, *21*, 386.

Table 2. ^{1}H NMR Chemical Shifts (ppm) for Diamagnetic Systems[a]

					meso-phenyl								
	pyrrole				*o*-H		*m*-H		*p*-H		*p*-OCH_3		
compound	a	b	c, d	*meso*	A	B	A	B	A	B	A	B	NH
$TrPPH_2$	9.32	8.99	8.84, 8.87	10.20	8.15−8.25		7.7−7.8		7.7−7.8		−		−3.03
$(TrPP)Zn^{II}$	9.38	9.07	8.94, 8.97	10.24	8.15−8.25		7.7−7.8		7.7.−7.8		−		−
$(TrPP)Ga^{III}Cl$	9.51	9.22	9.10, 9.11	10.41	8.0−8.4		7.65−7.9		7.65−7.9		−		−
$(Tr(p\text{-MeOP})P)Zn^{II}$	9.36	9.09	8.97, 8.98	10.21	8.08−8.14		7.23−7.29		−		4.09	4.07	−
$(TrPPH_2)_2$	8.04	8.55	8.87, 8.89	−	8.15−8.21	8.23−8.28	7.60−7.66	7.75−7.81	7.60−7.66	7.75−7.81	−		−2.25
$(TrPPH_2)$	8.03	8.56	8.88, 8.91	−	8.16−8.22	8.25−8.28	7.62−7.67	7.75−7.80	7.62−7.67	7.75−7.80			−2.22
$(Tr(p\text{-MeOP})PH_2)$	8.05	8.58	8.90, 8.94		8.10	8.17	7.17	7.31			3.98	4.11	−2.25
$(Tr(p\text{-MeOP})PH_2)_2$	8.03	8.57	8.89, 8.91	−	8.09	8.17	7.17	7.32	−		3.97	4.11	−2.22
$(TrPP)_2Zn^{II}{}_2$	8.08	8.63	8.96, 8.99	−	8.17−8.20	8.25−8.28	7.62−7.64	7.75−7.80	7.62−7.64	7.75−7.80	−		−
$[(TrPP)Zn^{II}]$	8.07	8.62	8.96, 8.99	−	8.27−8.30	8.36−8.39	7.65−7.76	7.84−7.87	7.65−7.76	7.84−7.87			−
$[(Tr(p\text{-MeOP})P)Zn^{II}]$	8.08	8.65	8.98, 9.02		8.16	8.24	7.16	7.30			3.97	4.10	
$(Tr(p\text{-MeOP})P)_2Zn^{II}{}_2$	8.07	8.65	8.98, 9.02	−	8.10	8.18	7.16	7.30	−		3.97	4.11	
$(TrPP)_2(Ga^{III}Cl)_2$	8.14	8.75	9.10, 9.15	−	7.95−8.15		7.5−7.9		7.5−7.9		−		−
	8.53	8.88	9.11, 9.16		8.2−8.4								
$(TrPP)_2(In^{III}Cl)_2$	8.19	8.78	9.09, 9.13	−	8.0−8.2		7.5−7.9		7.5−7.9		−		−
	8.21	8.79	9.10, 9.12		8.3−8.5								

[a] Resonances labeled as in Figures 2 and 3.

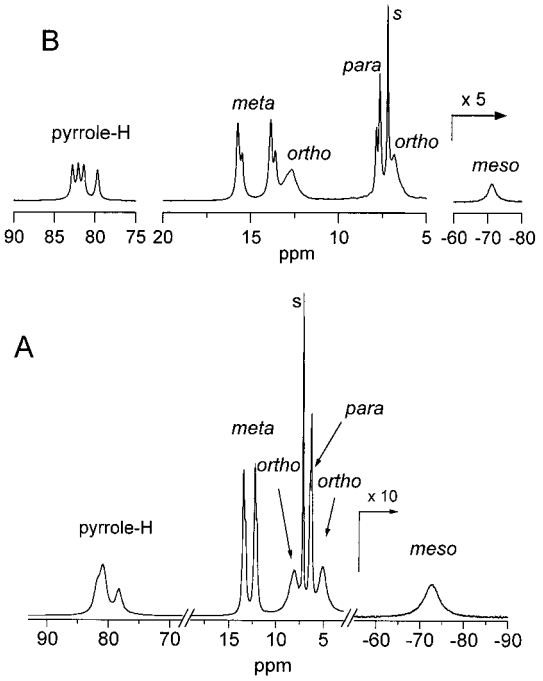

Figure 4. 300 MHz ^{1}H NMR spectrum of $(TrPP)Fe^{III}Cl$ (A) and $(TrPP)Fe^{III}I$ (B) in chloroform-*d* solution at 293 K. Resonance assignment: pyrrole-H, pyrrole proton resonances; *ortho*, *meta*, or *para* signals of *meso*-phenyl protons; *meso*, *meso*-H peak; s, solvent.

signal (Table 3). The position of the *meso* resonances is consistent with that found for $(OEP)Fe^{III}Cl$ ($\delta_{iso} = -55.6$ ppm),[11a] although the effect is markedly larger. The multiplicity and positions of the *meso*-phenyl resonances are consistent with the structure of the complex. In the series Cl^-, Br^-, I^- we have observed a systematic downfield change of the resonance positions related to the corresponding modification of the dipolar effect.[20]

Treatment of $(TrPP)Fe^{III}X$ with K_2CO_3 in water resulted in formation of $[(TrPP)Fe^{III}]_2O$. A set of three pyrrole resonances [13.2 (4H), 13.4 (4H), 13.6 ppm (8H)] reflects the symmetry of the subunit. The spectral properties resemble those of $(TPP)Fe^{III}O$.[22] The *meso* (20-H) resonance has been detected at $\delta = 6.3$ ppm, which corresponds to 5.5 ppm (29 °C) determined for $[(OEP)Fe^{III}]_2O$.[21]

The ^{1}H NMR spectra of $(TrPP)_2(Fe^{III}X)_2$ and $(Tr(p\text{-MeOP})P)_2(Fe^{III}X)_2$ have been analyzed in the context of the appropriate symmetry previously described for $(TrPP)_2(Ga^{III}Cl)_2$. Thus, the eight unequivalent pyrrole positions should produce eight downfield-shifted pyrrole resonances. In addition one can expect six *ortho*, six *meta*, and three *para* or *p*-methoxyphenyl signals. Additional differentiation of subunits in $[(TrPP)Fe^{III}X][(Tr(p\text{-MeOP})P)Fe^{III}X]$ doubles the predicted number of resonances. The representative ^{1}H NMR spectra of high-spin complexes $[(TrPP)Fe^{III}Cl][(Tr(p\text{-MeOP})P)Fe^{III}Cl]$ and $[(TrPP)Fe^{III}I][(Tr(p\text{-MeOP})P)Fe^{III}I]$ are presented in Figure 5. Table 3 contains further data for a wider range of complexes. In general, the observed line width of $(TrPP)_2(Fe^{III}X)_2$ increases, as expected for high-spin iron porphyrins, in the order $I^- < Br^- < Cl^-$.[11,20] Because of this trend, it has been expeditious to examine data for the iodide complexes, since these have the narrowest, and consequently the best resolved, resonances. In particular, two broad pyrrole resonances located above 80 ppm are not readily observed for chloride derivatives, and only one asymmetric pyrrole signal is visible (Figure 5). The presence of two paramagnetic centers produces marked variation of the pyrrole line widths. The effect has been clearly demonstrated for iodide derivatives. The $(TrPP)_2(Fe^{III}I)_2$ spectrum reveals a multiplet of six unequivalent pyrrole resonances centered at 80 ppm and two well-separated although relatively broad resonances corresponding to a (88.7 ppm, $\Delta\nu_{1/2} \cong 700$ Hz) and a′ (83.9 ppm, $\Delta\nu_{1/2} \cong 500$ Hz) (Figure 6, trace A). The line widths of the remaining six pyrrole resonances are markedly smaller (ca. 200 Hz). As expected, six well-resolved *meta meso*-phenyl resonances of $(TrPP)_2(Fe^{III}I)_2$ have been identified at the 12−16 ppm region (Table 3). Their number is doubled for $[(TrPP)Fe^{III}I][(Tr(p\text{-MeOP})P)Fe^{III}I]$ as shown in an expansion of this region (Figure 5).

The line widths have been used to correlate some of the pyrrole resonances with the proton location in the dimeric structure. The dipolar contribution to line width broadening is presumed to be proportional to r^{-6}, where r is the distance from the paramagnetic center to the proton in question when ligand-centered dipolar relaxation is insignificant.[23,24] The contribution

(21) La Mar, G. N.; Eaton, G. R.; Holm, R. H.; Walker, F. A. *J. Am. Chem. Soc.* **1973**, *95*, 63.
(22) La Mar, G. N.; Walker, F. A. *J. Am. Chem. Soc.* **1973**, *95*, 6950.
(23) Arasasingham, R. D.; Balch, A. L.; Cornman, C. R.; de Ropp, J. S.; Eguchi, K.; La Mar, G. N. *Inorg. Chem.* **1990**, *29*, 1847.

Table 3. ^{1}H NMR Chemical Shifts (ppm) for High-Spin Iron(III) Porphyrins[a]

			meso-phenyl			
compound	pyrrole	*meso*	*o*-H	*m*-H	*p*-H	*p*-OCH_3
$(TrPP)Fe^{III}Cl$	78.5 (2H), 81.1 (4H), 81.9 (2H)	−72.4	5.1 (3H), 8.2 (3H)	12.1, 12.3 (2H), 13.3, 13.5 (2H)	6.4 (2H), 6.5	−
$(TrPP)Fe^{III}Br$	79.4 (2H), 81.5 (2H), 81.9 (2H), 82.6 (2H)	−72.3	5.6 (3H), 9.8 (3H)	12.8, 13.0 (2H), 14.2, 14.5 (2H)	7.0 (2H), 7.1	−
$(TrPP)Fe^{III}I$	79.7 (2H), 81.4 (2H), 82.1 (2H), 82.8 (2H)	−66.5	6.9 (3H), 12.7 (3H)	13.6, 13.9 (2H), 15.5, 15.8 (2H)	7.7 (2H), 7.9	−
$[(TrPP)Fe^{III}]_2O$	13.2 (4H), 13.4 (4H), 13.6 (8H)	6.3 (2H)	7−8	7−8	7−8	−
$(TrPP)_2(Fe^{III}Cl)_2$	∼80.8 (16H)[b]	−	∼5.5 (6H), ∼8.5 (6H)	11.9 (4H), 12.3 (2H), 13.1 (4H), 13.5 (2H)	6.0 (2H), 6.2 (2H), 6.0 (2H)	−
$[(TrPP)Fe^{III}Cl][(Tr(p$-MeOP)P)$Fe^{III}Cl]$	∼80.5 (16H)[b]	−	∼5.1 (6H), ∼8.1 (6H)	11.5 (2H), 11.8 (3H), 12.2, 12.5 (2H), 13.0 (3H), 13.6	5.9, 6.1, 6.7	4.7 (3H), 4.9 (3H), 5.3 (3H)
$(Tr(p$-MeOP)P$)_2(Fe^{III}Cl)_2$	∼80.8 (16H)[b]	−	∼5 (6H), ∼8 (6H)	11.4 (4H), 11.8 (2H), 12.5 (4H), 13.0 (2H)	−	4.7 (3H), 4.8 (3H), 5.3 (3H)
$(TrPP)_2(Fe^{III}Br)_2$	81.9 (14H), 84.9, 88.1	−	∼5.8 (6H), ∼10.3 (6H)	12.4, 12.6, 13.1, 13.8, 14.1, 14.7 (2H each)	6.2 (2H), 6.6 (2H), 7.2 (2H)	−
$(TrPP)_2(Fe^{III}I)_2$	80.4, 80.9, 81.1 (12H); 83.2, 83.8, 88.7 (2H)	−	∼7 (6H), ∼13 (6H)	13.0, 13.3, 14.0, 14.8, 15.1, 16.0 (2H each)	6.9 (2H), 7.3 (2H), 8.3 (2H)	−
$[(TrPP)Fe^{III}I][(Tr(p$-MeOP)P$)Fe^{III}I]$	80.6, 81.6 (12H); 84.0 (2H), 89.2 (2H)	−	∼7 (6H), ∼13 (6H)	12.6, 13.0, 13.3, 13.6, 14.0, 14.3, 14.6, 14.8, 15.2, 15.4, 16.0[c]	7.6, 7.7, 8.3	5.2 (3H), 5.6 (3H), 6.5 (3H)

[a] Chloroform-*d*, 293 K. [b] Asymmetric line composed from few components. [c] Intensities not determined, their sum equals 12H.

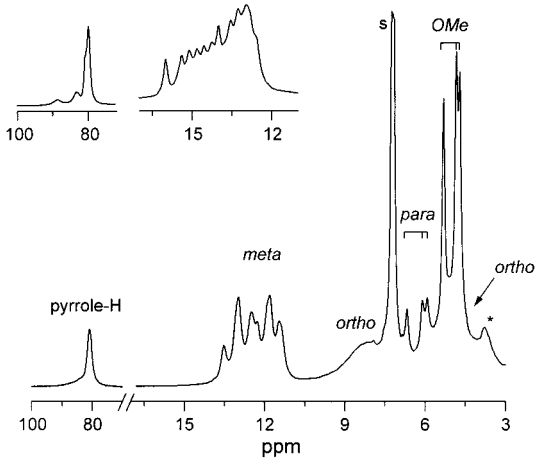

Figure 5. ^{1}H NMR spectrum of $[(TrPP)Fe^{III}Cl][(Tr(p$-MeOP)P$)Fe^{III}Cl]$ in chloroform-*d* solution at 293 K (OMe, *p*-OCH_3 resonances). Insets present the pyrrole and *meta*-H regions of $[(TrPP)Fe^{III}I][(Tr(p$-MeOP)-P$)Fe^{III}I]$.

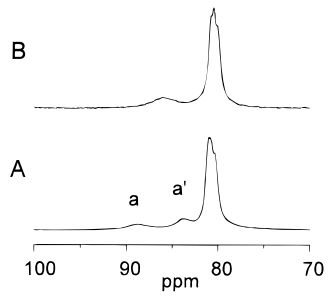

Figure 6. ^{1}H NMR spectrum of $(TrPP)_2(Fe^{III}I)_2$ (pyrrole region) in chloroform-*d*, 293 K (A). Trace B presents ^{1}H NMR spectrum from the same solution after addition of the excess of TBAI. Labeling of resonances is consistent with Scheme 2.

from the internal iron(III) ion via dipolar and scalar mechanisms has been approximated by the line widths of pyrrole resonances centered at 80 ppm which vary over a rather narrow range (ca. 200 Hz). The markedly larger line widths of a and a′ protons can be split into two parts: the internal one, which is identical as for other pyrrole positions, and the remaining external one. The most likely the external contribution derives mainly from the dominant dipolar contribution of the closely located external iron(III) ion. Considering the relative position of the a and a′ protons relative to the external iron(III) ($r_a < r_{a'}$), the broadest resonances could be unambiguously assigned. The downfield shift of a and a′ resonances upon the dimer formation can be tentatively explained by placement of these protons in the dipolar shift deshielding zone produced by the neighboring iron(III) porphyrin. With the iron(III) ion displaced from the porphyrin plane, the effect is more pronounced for the a proton.

The collapse of the a, a′ doublet upon addition of I^- in the form of TBAI is illustrated in Figure 6. These changes are accompanied by the parallel simplification of the other spectral regions. Consequently the three pyrrole resonances that are discernible around 80 ppm are assigned to the collapsed pairs b and b′, c and c′, and d and d′, respectively. Accordingly the multiplet of six *m*-phenyl resonances simplifies to two lines with the 2:1 intensity ratio. As the result, the NMR spectrum of $(TrPP)_2(Fe^{III}I)_2$ presents the features expected for the higher effective symmetry described already for $(TrPP)_2Zn^{II}_2$. To account for the observed phenomenon, we suggest that the associative mechanism described in Scheme 2 is operative. All pairs do average since the activated $[(TrPP)Fe^{III}I_2]^-$ subunit has the plane of symmetry through the porphyrin skeleton. The analogous mechanism was presented previously for the (TPP)-$Fe^{III}X$ systems.[25] This process also results in a mutual interconversion of the iron(III) diporphyrin enantiomers.

The chromatography of $(TrPP)_2(Fe^{III}X)_2$ on a basic alumina column or methathesis by stirring of its dichloromethane (benzene) solution with an excess of sodium hydroxide results in replacement of the halo ligands with hydroxy groups. The ^{1}H NMR spectra indicate that the product contains both (TrPP)-Fe^{III}(OH) and $-(TrPP)Fe^{III}OFe^{III}(TrPP)-$ moieties, although the

(24) Swift, J. In *NMR of Paramagnetic Molecules*; La Mar, G. N., Horrocks, W. D., Jr., Holm, R. H., Eds.; Academic Press: New York; 1973; p 53.

(25) (a) La Mar, G. N. *J. Am. Chem. Soc.* **1973**, *95*, 1662. (b) La Mar, G. N.; Saterlee, J. D.; Snyder, J. *J. Am. Chem. Soc.* **1974**, *96*, 7137. (c) Snyder, R. V.; La Mar, G. N. *J. Am. Chem. Soc.* **1977**, *98*, 4419.

Scheme 2

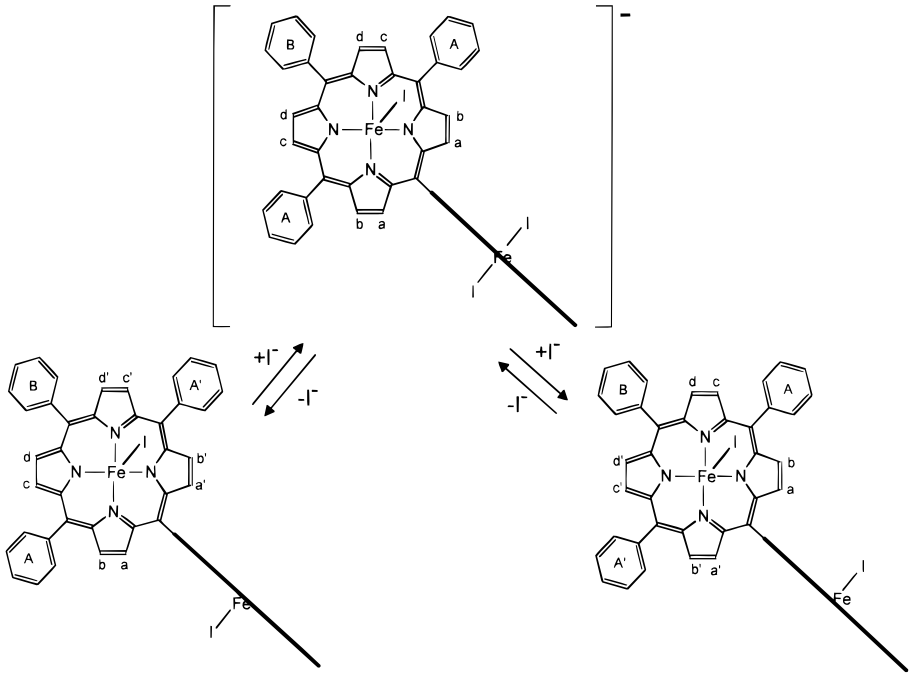

Scheme 3

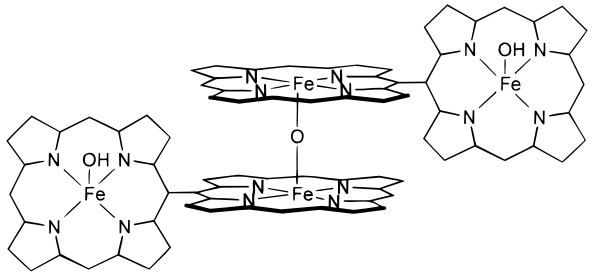

relative amounts of two fragments vary. The $(TrPP)Fe^{III}(OH)$ element has been identified by the very broad pyrrole resonance at 81.3 ppm and *m*-phenyl signals at 12.3 and 13.5 ppm. In particular, the pyrrole resonance is essentially broader than the resonance of the precursor, $(TrPP)_2(Fe^{III}Cl)_2$, as expected for the hydroxy coordination.[26] The set of resonances at ca. 14 ppm (293 K), which show anti-Curie behavior of the isotropic shift, has been assigned to the μ-oxo bridged fragment $-(TrPP)Fe^{III}$-$OFe^{III}(TrPP)-$. These observations are consistent with the initial formation of $(TrPP)_2(Fe^{III}(OH))_2$, accompanied by eventual generation of dimeric (oligomeric) species linked by the μ-oxo bridge(s). The two terminal subunits remain five-coordinate with the OH group in the axial position, as shown in the Scheme 3. The steric constraints of the diporphyrin exclude the formation of the cyclic $(TrPP)_2(Fe^{III}OFe^{III})_2(TrPP)_2$ complex with two μ-oxo bridges linking subunits of two iron diporphyrins.

Low-Spin Iron Porphyrins—NMR Studies. Addition of an excess of potassium cyanide to a solution of $(TrPP)Fe^{III}Cl$, $(TrPP)_2(Fe^{III}Cl)_2$, or{$[(TrPP)Fe^{III}Cl][(Tr(p\text{-}MeOP)P)Fe^{III}Cl]$} in methanol-$d_4$ results in their conversion to six-coordinate low-spin complexes: $[(TrPP)Fe^{III}(CN)_2]^-$, $[(TrPP)_2(Fe^{III}(CN)_2)_2]^{2-}$, and $\{[(TrPP)Fe^{III}(CN)_2][(Tr(p\text{-}MeOP)P)Fe^{III}(CN)_2]\}^{2-}$. Representative ^{1}H NMR spectra are shown in Figure 7. Relevant chemical shift data are given in Table 4. The characteristic sets of four upfield-shifted pyrrole resonances are observed for $[(TrPP)Fe^{III}(CN)_2]^-$ and $[(TrPP)_2(Fe^{III}(CN)_2)_2]^{2-}$. Eight signals in this spectral region are found for $\{[(TrPP)Fe^{III}(CN)_2][(Tr(p\text{-}MeOP)P)Fe^{III}(CN)_2]\}^{2-}$. These signals are accompanied by sets of upfield shifted *ortho* and *para meso*-phenyl proton resonances and downfield shifted *meta* signals. The *meso*-H peak has been observed at $\delta = -6.9$ ppm (293 K) for $[(TrPP)Fe^{III}(CN)_2]^-$. The isotropic shift of the pyrrole resonances is consistent with the $(d_{xy})^2(d_{xz},d_{yz})^3$ ground electronic state.[11] The necessary assignments required an application of two-dimensional NMR techniques, ^{1}H COSY and NOESY,[12a] and the results are shown in Figure 7 and Table 4. The multiplicity of resonances is consistent with the symmetry analysis presented previously. The presence of two paramagnetic centers in $[(TrPP)_2(Fe^{III}(CN)_2)_2]^{2-}$ and $\{[(TrPP)Fe^{III}(CN)_2][(Tr(p\text{-}MeOP)P)Fe^{III}(CN)_2]\}^{2-}$ is not reflected in the essential changes of the isotropic shifts. However, the analytically important broadening of resonances has been evidently observed. Thus, the four pyrrole signals of monomeric $[(TrPP)Fe^{III}(CN)_2]^-$ display the similar line widths. In contrast, selective broadening of the a proton resonance of $[(TrPP)_2(Fe^{III}(CN)_2)_2]^{2-}$ is observed ($\Delta\nu_{1/2} \cong 20$ Hz, for three others 12−14 Hz). Because of the proximity of the pyrrolic a protons to the iron ion in the adjacent molecule, these protons are strongly affected by dipolar relaxation from that paramagnetic center. An analogous effect has been observed for $\{[(TrPP)Fe^{III}(CN)_2][(Tr(p\text{-}MeOP)P)Fe^{III}(CN)_2]\}^{2-}$ (Figure 7) where the a and a′ resonances are selectively broadened. This spectrum consists of a superposition of the separate patterns of two different subunits. The first set of $[(TrPP)Fe^{III}(CN)_2]^-$ resonances shows chemical shifts in the range found for $[(TrPP)_2(Fe^{III}(CN)_2)_2]^{2-}$. The unambiguous assignment of a and a′ resonances because of their broadening served as a convenient starting point of the NOESY correlation, resulting in the full assignment of the heterogeneous iron(III) diporphyrin.

Iron Porphyrin Cation Radicals—NMR Investigations. The oxidation of $(TrPP)_2(Fe^{III}Cl)_2$ has been monitored by ^{1}H NMR spectroscopy. The phenoxatiin cation radical in the form of the hexachloroantimonium(V) salt $(Phox^{\bullet})(SbCl_6)$ has been used as the one-electron oxidant. This species is known to oxidize iron(III) complexes, e.g. $(TTP)Fe^{III}Cl$, to iron(III)

(26) Cheng, R.-J.; Latos-Grażyński, L.; Balch, A. L. *Inorg. Chem.* **1982**, *21*, 2412.

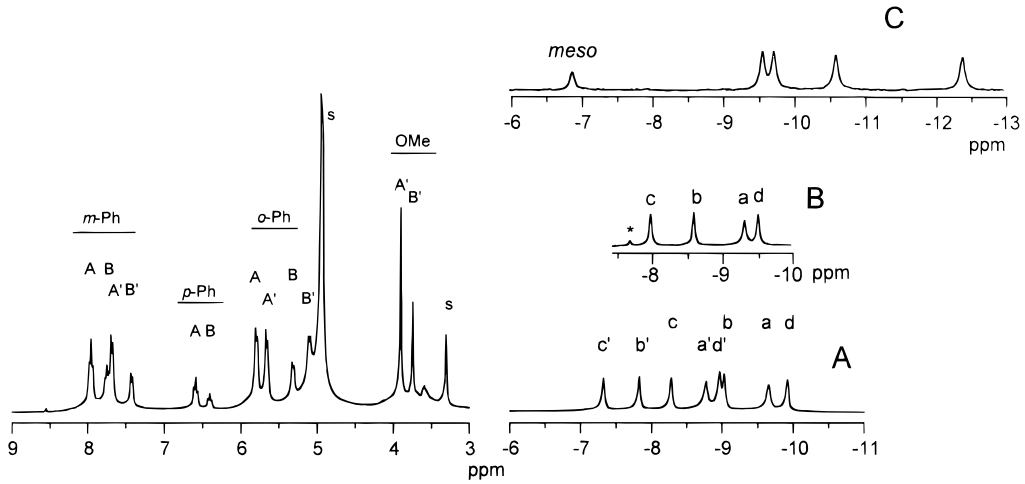

Figure 7. ^{1}H NMR spectrum of $\{[(TrPP)Fe^{III}(CN)_2][(Tr(p\text{-}MeOP)P)Fe^{III}(CN)_2]\}^{2-}$ in methanol-d_4 solution at 293 K (trace A). Resonances of $[(Tr(p\text{-}MeOP)P)Fe^{III}(CN)_2]^-$ fragment labeled with ′. Insets present the upfield part of the spectra of $[(TrPP)_2(Fe^{III}(CN)_2)_2]^{2-}$ (B) and $[(TrPP)Fe^{III}(CN)_2]^-$ (C).

Table 4. ^{1}H NMR Chemical Shifts (ppm) for Low-Spin Iron(III) Porphyrins[a,b]

						meso-phenyl							
	pyrrole					*o*-H		*m*-H		*p*-H		*p*-OCH_3	
compound	a	b	c	d	*meso*	A	B	A	B	A	B	A	B
$[(TrPP)Fe^{III}(CN)_2]^-$	(−9.5 and −12.3), (−9.7 and −10.5)				−6.9	6.1	5.1	7.8	7.3	6.7	6.4	−	
$[(TrPP)_2(Fe^{III}(CN)_2)_2]^{2-}$	−9.4	−8.6	−8.0	−9.6	−	5.8	5.3	8.0	7.8	6.6	6.4	−	
$\{[(TrPP)Fe^{III}(CN)_2]$	−9.6	−9.0	−8.2	−9.9	−	5.8	5.3	8.0	7.8	6.8	6.4		
$[(Tr(p\text{-}MeOP)P)Fe^{III}(CN)_2]\}^{2-}$	−8.7	−7.8	−7.3	−8.9		5.7	5.1	7.7	7.4			3.9	3.7

[a] Methanol-d_4, 293 K. [b] Labeling follows that in Figure 3.

complexes of porphyrin π-cation radicals, e.g. $[(TTP^{\bullet})Fe^{III}Cl](SbCl_6)$.[27] Figure 8 shows the relevant spectra from the reaction between $(TrPP)_2(Fe^{III}Cl)_2$ and a dichloromethane solution of $(Phox^{\bullet})(SbCl_6)$. Trace A shows the spectrum of $(TrPP)_2(Fe^{III}Cl)_2$ alone. Traces B and C present the spectrum after the additions of successive aliquots of oxidant. The titration results in smooth changes of the chemical shifts to achieve characteristic asymptotic values for each set of resonances, facilitating their assignment. Thus, the pattern typical for iron(III) porphyrin π-cation radical is observed which resembles the ^{1}H NMR spectrum of $[(TPP^{\bullet})Fe^{III}Cl](SbCl_6)$. However, the paramagnetic shift changes of *meso* phenyl resonances upon one-electron oxidation to give $[(TrPP)_2(Fe^{III}Cl)_2](SbCl_6)$ are roughly one-half that expected for a monomeric porphyrin: the *ortho*-H signal is observed at 24 ppm, *para*-H at 19 ppm, and *meta*-H at −2 ppm. Some differentiation of the pyrrole resonances has been noted as well, although they remain centered around 80 ppm (Figure 8). Addition of further $(Phox^{\bullet})(SbCl_6)$ does not alter the spectrum assigned to $[(TrPP)_2(Fe^{III}Cl)_2](SbCl_6)$. However, a new set of resonances grows while the lines of $[(TrPP)_2(Fe^{III}Cl)_2](SbCl_6)$ gradually diminish in intensity. The new multiplets assigned to the *meso*-phenyls appear in the regions overlapping with those determined for $[(TPP^{\bullet})Fe^{III}Cl](SbCl_6)$. The pyrrole resonances are split to form a complex set located at ca. 80 ppm and accompanied by two strongly shifted sets of resonances at 95 and 115 ppm, assigned to a and a′ pyrrole protons (trace D). The broader components can be attributed to axial ligand replacement, although the identity of the ligands could not be determined. On the basis of the similarity of patterns of resonances we ascribe new features in the ^{1}H NMR spectrum to the formation of $[(TrPP^{\bullet})_2(Fe^{III}Cl)_2]^{2+}$, which contains two five-coordinate $[(TrPP^{\bullet})Fe^{III}Cl]^+$ subunits. Thus, as reflected by the multiplicity of resonances, the molecular structure of $[(TrPP^{\bullet})_2(Fe^{III}Cl)_2]^{2+}$ retains the characteristic geometry of the unoxidized precursor $[(TrPP)_2(Fe^{III}Cl)_2]$ shown in Scheme 2. For instance, the a and a′ protons, located in the proximity of the bridging fragment, revealed the 20 ppm chemical shift difference due to the five-coordinate geometry of the iron(III). The correlation between the molecular geometry of metallodiporphyrins and spectroscopic consequences has been analyzed in the previous sections. In both cases, i.e., $[(TrPP)_2(Fe^{III}Cl)_2](SbCl_6)$ and $[(TrPP^{\bullet})_2(Fe^{III}Cl)_2](SbCl_6)_2$, the oxidation can be reversed by treating the oxidized solution with zinc dust to regenerate $(TrPP)_2(Fe^{III}Cl)_2$.

The spectroscopic data indicate that $(TrPP)_2(Fe^{III}Cl)_2$ can undergo two reversible one-electron oxidations to form $[(TrPP)_2(Fe^{III}Cl)_2]^+$ and $[(TrPP^{\bullet})_2(Fe^{III}Cl)_2]^{2+}$. In solution, electron exchange between $(TrPP)_2(Fe^{III}Cl)_2$ and $[(TrPP)_2(Fe^{III}Cl)_2]^+$ is sufficiently rapid to result in a single, population-averaged set of ^{1}H NMR resonances. In contrast, the rate of electron exchange between $[(TrPP)_2(Fe^{III}Cl)_2]^+$ and $[(TrPP^{\bullet})_2(Fe^{III}Cl)_2]^{2+}$ is sufficiently slow so that resonances from each component are clearly resolved (as seen in Figure 8, trace D). The pattern of resonances of $[(TrPP)_2(Fe^{III}Cl)_2]^+$ is similar in several ways to that of $[(TPP^{\bullet})Fe^{III}Cl]^+$.[27] The observed features are consistent with presence of a ligand-based a_{2u} radical antiferromagnetically coupled to the high-spin iron(III) center.[27] Thus the initial one-electron oxidation generates the product that contains two iron(III) centers, one $(TrPP)^{2-}$ ligand and one oxidized $(TrPP^{\bullet})^-$. The observation of one set of triphenylporphyrin resonances instead of two separate sets (one corresponding to $(TrPP)Fe^{III}Cl$ and one to $[(TrPP^{\bullet})Fe^{III}Cl]^+$) may indicate that the two fragments are equivalent. Consequently, the ligand-based unpaired electron must be delocalized over both macrocycles. Alternatively, the

(27) Gans, P.; Buisson, G.; Duée, E.; Marchon, J.-C.; Erler, B. S.; Scholz, W. F.; Reed, C. A. *J. Am. Chem. Soc.* **1986**, *108*, 1223.

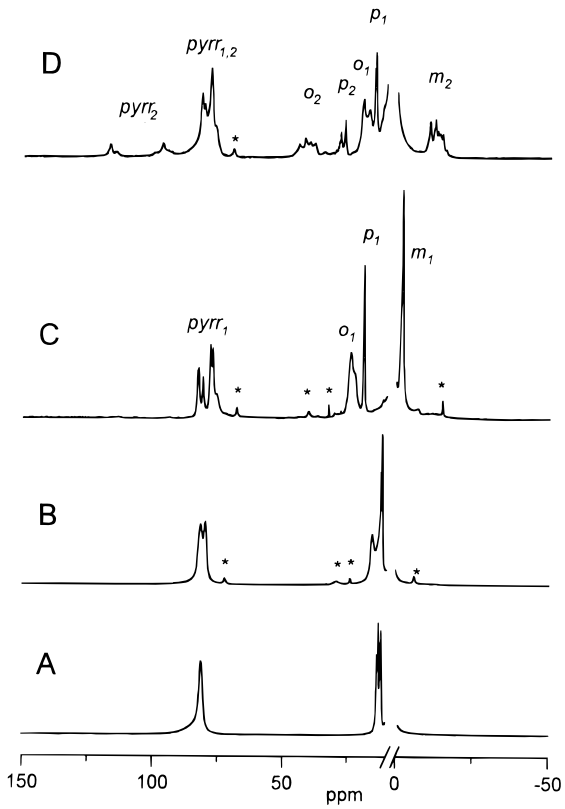

Figure 8. ^{1}H NMR spectra of $(TrPP)_2(Fe^{III}Cl)_2$ with $(Phox^{\bullet})(SbCl_6)$ in dichloromethane-d_2 (295 K): trace A, $(TrPP)_2(Fe^{III}Cl)_2$; traces B, C, after addition of succesive alliquots of $(Phox^{\bullet})(SbCl_6)$ in dichloromethane-d_2; trace D was obtained by overnight oxidation of $[(TrPP)_2(Fe^{III}Cl)_2]$ with the slurry of $(Phox^{\bullet})(SbCl_6)$. Signals of $[(TrPP)_2(Fe^{III}Cl)_2]^+$ and $[(TrPP^{\bullet})_2(Fe^{III}Cl)_2]^{2+}$ labeled with 1 and 2, respectively. Resonances of residual $[(TPP^{\bullet})Fe^{III}Cl]^+$ are identified by asterisks. The 0−10 ppm region of all spectra was omitted from the figure.

internal exchange of the unpaired electron between two structural fragments of $[(TrPP)_2(Fe^{III}Cl)_2]^+$ must be very fast (eq 1)

$$[(TrPP^{\bullet})Fe^{III}Cl][(TrPP)Fe^{III}Cl]^+ \rightleftharpoons [(TrPP)Fe^{III}Cl][(TrPP^{\bullet})Fe^{III}Cl]^+ \quad (1)$$

As the partial consequences of this delocalization, the paramagnetic shifts for the *meso*-phenyl resonances of $[(TrPP)_2(Fe^{III}Cl)_2]^+$ are smaller than those for $[(TrPP^{\bullet})_2(Fe^{III}Cl)_2]^{2+}$, in which each macrocyle is oxidized by one electron. The extensive delocalization of the positive hole that is seen for $[(TrPP)_2(Fe^{III}Cl)_2]^+$ is of interest in the context of the electron/energy transfer using the polyporphyrinic *meso*−*meso*-linked arrays.

We can conclude that the proximity of two π-electronic systems of porphyrinic subunits linked by a *meso*−*meso* bridge facilitates the delocalization of the radical π spin density over two macrocyclic fragments. One has to keep in mind that the two porphyrinic systems can accept several nonorthogonal orientations of the porphyrin planes. Molecular motion about the *meso*−*meso* link allows the direct overlap of π-orbitals. Previously it was shown that direct *meso*−*meso* connectivity resulted in the strong excitonic splitting in the Soret bands of $(TrPP)_2Zn^{II}_2$.[10]

The extensive delocalization of the ligand hole was previously observed for other dimeric iron(III) porphyrin complexes such as $\{[(TPP)Fe^{III}]_2O\}^+$ and $\{[(OEPO)Fe^{III}]_2\}^+$, although their delocalization pathways are fundamentally different.[15,28,29] The proximity of porphyrin planes situated one above the other and/or the contribution of the Fe−O linkage was considered to be quite significant in providing a conjugative path for delocalization.[15]

Two-electron oxidation results in $[(TrPP^{\bullet})_2(Fe^{III}Cl)_2]^{2+}$, where two iron(III) porphyrin π-cation radicals are located in close proximity. Formally the system contains four centers of magnetism, which opens a route to a rather complex pattern of magnetic interactions. However, the mutual interaction between subunits is rather small since the paramagnetic shifts resemble those for monomeric $[(TPP^{\bullet})Fe^{III}Cl]^+$, but with the significant exception of a and a′ resonances. Thus paramagnetic shifts of a and a′ reflect simultaneously a contribution of all four magnetic centers, namely, the iron(III) center, the cation radical localized on the porphyrin, the iron(III) center of the adjacent porphyrin, and the porphyrin cation radical of the adjacent porphyrin. The contribution of the cation radical of one subunit to the paramagnetic shift of the second one can be evaluated by assuming the simple additivity of the contributions. Since the formation of the cation radical has the rather minor influence on the shift of the remaining pyrrolic protons, as expected for the a_{2u} ground electronic state, we have assumed that the difference in the shifts seen for $[(TrPP^{\bullet})_2(Fe^{III}Cl)_2]^{2+}$ and $(TrPP)_2(Fe^{III}X)_2$ results solely from the factor of interest (the relevant lines of $(TrPP)_2(Fe^{III}Cl)_2$ were too broad to be observed, so the corresponding values for $(TrPP)_2(Fe^{III}Br)_2$ have been considered). Accordingly, the pertinent factors are equal to 26 and 11 ppm. At the present stage, the interpretation of these changes is rather difficult, as they may reflect either the additional contribution of the π-spin density and/or the modification of external contribution to the dipolar shifts.

Conclusions

meso−*meso*-Linked diporphyrin presents the simplest example of porphyrin arrays where the porphyrinic fragments are linked via *meso*−*meso* positions without any spacer. In our investigations we have focused on the hexaphenyl derivative of the 5,5′-bisporphyrin. The ligand of interest can be formally treated as the product of the replacement of one of the phenyls of tetraphenylporphyrin with another type of aromatic substituent, i.e., the triphenylporphyrin moiety. To trace the extent of communication between two closely linked porphyrinic fragments, we have decided to explore the differences in the paramagnetic shift pattern of those seen for iron(III) diporphyrins $(TrPP)_2(Fe^{III}Cl)_2$ and the corresponding monomeric species $(TrPP)Fe^{III}Cl$. As the mechanisms of the spin density distribution are directly related to the spin/electronic state of the iron porphyrin, we have extended ^{1}H NMR investigations on the representative states of iron(III) diporphyrins. Therefore, ^{1}H NMR spectra of iron(III) diporphyrin linked by the direct *meso*−*meso* bond have been investigated for the following spin/oxidation states: $(TrPP)_2(Fe^{III}Cl)_2$ (high spin); $[(TrPP)_2(Fe^{III}(CN)_2)_2]^{2-}$ (low spin); $[(TrPP)_2(Fe^{III}Cl)_2]^+$ (high-spin iron(III), diporphyrin radical); and $[(TrPP^{\bullet})_2(Fe^{III}Cl)_2]^{2+}$(high spin iron(III), diradical of diporphyrin). Generally, ^{1}H NMR investigation indicated that the interactions between two subunits of the diporphyrins are relatively small. As a matter of fact, the iron(III) diporphyrins $(TrPP)_2(Fe^{III}Cl)_2$, $[(TrPP)_2(Fe^{III}(CN)_2)_2]^{2-}$, and $[(TrPP^{\bullet})_2(Fe^{III}Cl)_2]^{2+}$ revealed the features which have been typically encountered in the spectra of the relevant monomeric complexes with one but very important exception. In the listed examples we have established the ^{1}H NMR "fingerprint" evidence of the

(28) Goff, H. M.; Phillippi, M. A. *J. Am. Chem. Soc.* **1982**, *104*, 6026.
(29) Arena, F.; Gans, P.; Marchon, J.-C. *Nouv. J. Chim.* **1985**, *9*, 505.

presence of the *meso*−*meso* link. Because of the proximity of the a and a′ protons to the iron(III) of the adjacent macrocycle, these protons are most strongly affected from the second paramagnetic center. Consequently, their signals are selectively broadened and in the case of high-spin complexes ($(TrPP)_2(Fe^{III}Br)_2$ and $(TrPP)_2(Fe^{III}I)_2$) and of diradical $[(TrPP^{\bullet})_2(Fe^{III}Cl)_2]^{2+}$ markedly downfield relocated from the position of other pyrrole resonances.

Importantly, the ^{1}H NMR spectrum of $[(TrPP)_2(Fe^{III}Cl)_2]^+$ indicated that a one-electron, ligand-based oxidation of $(TrPP)_2(Fe^{III}Cl)_2$ has occurred but the unpaired electron is delocalized over both *meso*−*meso*-linked macrocycles providing the crucial example of the very efficient unpaired spin density or electron transfer via the *meso*−*meso* bridge.

Experimental Section

Solvents and Reagents. All solvents were purified by standard procedures. Chloroform-*d* ($CDCl_3$, Cambridge Isotope Laboratories) was dried before use by passing through activated basic alumina. Methanol-d_4 and dichloromethane-d_2 (Cambridge Isotope Laboratories) were used as received. Phenoxatiinylium hexachloroantimonate [(Phox$^{\bullet}$)$(SbCl_6)$] was synthesized as previously described.[27]

Preparation of Compounds. 5,10,15-Triphenylporphyrin ($TrPPH_2$) and 5,10,15-tris(*p*-methoxyphenyl)porphyrin (Tr(*p*-MeOP)PH_2) have been obtained using the modification of the Lindsey method by methodology developed for mixed aldehyde−pyrrole condensation. Pyrrole (2 mL, 29 mmol), benzaldehyde (2.2 mL, 21.8 mmol), and paraformaldehyde (220 mg, 7.4 mmol) were dissolved in deoxygenated chloroform (600 mL). After addition of boron trifluoride etherate (0.3 mL), the reaction mixture was stirred in the dark and the solution was refluxed for 1 h. *p*-Chloranil (5.6 g) was added and the solution was refluxed for an additional 1h. The solution was then taken to dryness under reduced pressure by rotatory evaporation. The product was dissolved in dichloromethane and chromatographed on a basic alumina column to remove tarry products. Chromatography on activated basic alumina was than carried out. Two fractions containing tetraphenylporphyrin and 5,10,15-triphenylporphyrin were gradually eluted with benzene, evaporated to dryness, and recrystallized from *n*-octane/dichloromethane (1:1 v/v) to produce $TrPPH_2$ in yields of 5.5−7%. The spectroscopic characteristics correspond to those determined by Callot et al. for $TrPPH_2$ synthesized by the different procedure.[30]

(Tr(*p*-MeOP)PH_2) was obtained analogously (*p*-anisoaldehyde instead of benzaldehyde was used).

5,5′-Bis(10,15,20-triphenylporphyrin) [$(TrPPH_2)_2$] and 5,5′-bis-(10,15,20-tris(*p*-metoxyphenylporphyrin) [(Tr(*p*-MeOP)$PH_2)_2$] have been obtained by a regiospecific *meso*−*meso* coupling of the corresponding monomeric zinc(II) complexes, $(TrPP)Zn^{II}$ or $(Tr(p\text{-}MeOP)P)Zn^{II}$, followed by demetalation with HCl. The synthetic details are given below for a hybrid diporphyrin.

($TrPPH_2$)(Tr(*p*-MeOP)PH_2). $(TrPP)Zn^{II}$ (46.2 mg, 0.077 mmol) and $(Tr(p\text{-}MeOP)P)Zn^{II}$ (26.5 mg, 0.038 mmol) were dissolved in the mixture of 20 mL of dichloromethane and 15 mL of tetrahydrofuran. Thallium(III) trifluoroacetate (75 mg, 0.138 mmol, 1.2 equiv) in 5 mL of THF was added to this solution. The color changed immediately from pink to green-brown. The stirring was continued for 15 min. Silica was added to the solution and the reaction mixture was filtered through a bed of silica gel. Dichloromethane eluted a red fraction which was evaporated to dryness on the rotatory evaporator. The benzene solution of the solid residue was subjected to chromatography on a silca gel column (0.040−0.063 mm, 230−400 mesh, Merck). Elution with benzene gave subsequently three main fractions, $(TrPP)_2Zn^{II}_2$, $[(TrPP)Zn^{II}][(Tr(p\text{-}MeOP)P)Zn^{II}]$, and $(Tr(p\text{-}MeOP)P)_2Zn^{II}_2$, that were recovered as the solvent was removed under vacuum. The hybrid zinc dipoprhyrin was identified by ^{1}H NMR (details are given in Table 2) and mass spectrometry [ESI: *m/z* = 1292.5 (M^+, 90), 645.4 (M^{2+}, 100)]. The demetalation with concentrated HCl of $[(TrPP)Zn^{II}][(Tr(p\text{-}MeOP)P)Zn^{II}]$ yielded ($TrPPH_2$)(Tr(*p*-MeOP)PH_2) (8 mg).

Table 5. Crystal Data and Data Collection Parameters for $(Tr(p\text{-}MeOP))Zn^{II}\cdot 0.4CH_2Cl_2$

formula	$C_{41.40}H_{30.80}Cl_{0.80}N_4O_3Zn$
fw	726.03
color and habit	red hexagonal plate
crystal system	monoclinic
space group	*C*2/*c*
a, Å	47.744(9)
b, Å	9.090(2)
c, Å	15.571(2)
α, deg	90
β, deg	93.770(13)
γ, deg	90
V, Å^3	6743(2)
T, K	154(2)
Z	8
d_{calcd}, g cm^{-3}	1.430
radiation, Å	Cu Kα (1.541 78 Å)
μ, mm^{-1}	1.973
range of transm factors	0.71−0.91
no. unique data	4361
no. parameters refined	494
R[a]	0.076
wR2[b]	0.253

[a] $R = \sum||F_o| - |F_c||/\sum|F_o|$ (observed data, $I > 2\sigma(I) = 3179$). [b] wR2 $= [\sum[w(F_o^2 - F_c^2)^2]/\sum[w(F_o^2)^2]]^{1/2}$ (all data).

Metal Ion Insertions and Axial Ligand Methathesis. Insertion of zinc(II), iron(III), gallium(III), and indium(III) followed known routes.[13] Corresponding chloro, bromo, and iodo derivatives of iron(III) porphyrins (diporphyrins) were obtained by stirring the dichloromethane (benzene) solution of appropriate iron(III) porphyrin with an excess of sodium hydroxide to produce μ-oxo diiron complex or respective hydroxo complexes. The required derivatives were prepared by stirring the dichloromethane solution of the hydroxo (μ-oxo) species with 1 M aqueous HX (X = Cl, Br, I). The organic layer was separated, dried, and evaporated to dryness, yielding corresponding iron(III) high-spin complexes.

The dicyano-ligated complexes of the investigated iron(III) porphyrin were prepared by dissolution of 2−3 mg of the respective high-spin complex in 0.4 mL of methanol-d_4 saturated with KCN.

Oxidation of $(TrPP)_2(Fe^{III}Cl)_2$. Titrations were performed by the addition of aliquots of saturated solution of (Phox$^{\bullet}$)$(SbCl_6)$ in dichloromethane-d_2 by means of a microliter syringe to a solution of $(TrPP)_2(Fe^{III}Cl)_2$ in dichloromethane-d_2. The oxidizing reagent has limited solubility in dichloromethane-d_2. The concentrated solution of $[(TrPP^{\bullet})_2(Fe^{III}Cl)_2]^{2+}$ was obtained by overnight oxidation of $[(TrPP)_2(Fe^{III}Cl)_2]$ with the slurry of (Phox$^{\bullet}$)$(SbCl_6)$.

Molecular Mechanics Calculation. Molecular mechanics calculations using the HyperChem software (Autodesk) were carried out and displayed on a PC Pentium computer. The standard MM+ force field, with the constraints set on the coordination bonds to achieve a gallium(III) porphyrin geometry, have been used as described in the text.

Instrumentation. ^{1}H NMR spectra were recorded on a Bruker AMX spectrometer operating in the quadrature mode at 300 MHz. A typical spectrum was collected over a 45 000 Hz spectral window with 16K data points with 500−5000 transients for the experiment and a 50 ms relaxation delay. The free induction decay (FID) was apodized using exponential multiplication depending on the natural line width. This induced 5−50 Hz broadening. The residual ^{1}H NMR resonances of the deuterated solvents were used as secondary references. An inversion−recovery sequence was used to suppress the diamagnetic signals in the selected spectra. 2D COSY and NOESY experiments were carried out as described previously.[12] Mass spectra were recorded on a Finnigan MAT TSQ 700 spectrometer using the ESI technique.

X-ray Structure Determination. Crystals of $(Tr(p\text{-}MeOP)P)Zn^{II}\cdot 0.4CH_2Cl_2$ were prepared by diffusion of *n*-octane into a dichloromethane solution of the complex in a thin tube. Suitable crystal was

(30) Callot, H.; Schaeffer, E. *J. Chem. Res. (S)* **1978**, 51; *J. Chem. Res. (M)* **1978**, 0690.

coated with light hydrocarbon oil and directly mounted in the 130 K dinitrogen stream of the low-temperature apparatus.

X-ray Data Collections. Data were collected at 130 K on a Siemens P4 diffractometer that was equipped with a rotating anode source and a Siemens LT-2 low-temperature apparatus. Two check reflections showed random (less than 2%) variation during the data collection. The data were corrected for Lorentz and polarization effects. The radiation employed was Ni-filtered Cu Kα from a Siemens rotating-anode source operating at 15 kW. Crystal data are compiled in Table 5.

Solution and Structure Refinement. Calculations were performed on a PC with programs of SHELXTL version 5. Scattering factors for neutral atoms and corrections for anomalous dispersion were taken from the standard source.[31] The solutions were obtained by Patterson methods. The methoxy group C(28) to C(34) and O(2) is disordered over two sites. The major site was refined to 0.79 fractional occupancy. The C−O bond lengths within this group were fixed at 1.4 Å. Two sites, which overlapped in space, were occupied by dichloromethane molecules, which were defined by four chlorine atom positions at 0.20 fractional occupancy. Carbon atoms were not found for these two molecules. The largest peak in the final difference map (1.520 e $Å^{-3}$) is 0.902 from Cl(1) and 1.059 from Cl(4). Attempts to model this peak into the framework of the dichloromethane molecules were unsuccessful. All non-hydrogen atoms, except the minor component of the disordered methoxy group and Cl(2), were refined anisotropically. The hydrogen atoms were refined as a riding molecule with fixed isotropic thermal parameters. An empirical absorption correction, XABS2, was applied.[32]

Acknowledgment. The financial support of the Polish State Committee for Scientific Research KBN (Grant 3 T09A 155 15) and the U.S. National Institutes of Health (Grant GM 26226) is kindly acknowledged.

Supporting Information Available: Crystal data, atom coordinates, complete listings of bond lengths, anisotropic displacement coefficients and calculated hydrogen parameters. This material is available free of charge via the Internet at http://pubs.acs.org.

IC990038G

(31) *International Tables for X-ray Crystallography*; D. Reidel Publishing Co.: Boston, MA, 1991; Vol. C.

(32) Parkin, S.; Moezzi, B.; Hope, H. *J. Appl. Crystallogr.* **1995**, *28*, 53.